Local structure around Yb in $SrZr_{1-x}Yb_xO_3$



2001 J. Phys.: Condens. Matter 13 2455

(http://iopscience.iop.org/0953-8984/13/11/304)

INSTITUTE OF PHYSICS PUBLISHING JOURNAL OF PHYSICS: CONDENSED MATTER

J. Phys.: Condens. Matter **13** (2001) 2455–2466 www.iop.org/Journals/cm PII: S0953-8984(01)15688-2

# Local structure around Yb in $SrZr_{1-x}Yb_xO_3$

**O Kamishima, K Ohta, Y Chiba and T Hattori**

Research Institute for Scientific Measurements, Tohoku University, Sendai 980-8577, Japan

E-mail: kamisima@rism.tohoku.ac.jp

Received 20 July 2000, in final form 17 November 2000

**Abstract**

Local structures around Yb ions in the proton conductor Yb-doped $SrZrO_3$ have been investigated at room temperature by the EXAFS (extended x-ray absorption fine structure) technique. The radial structure functions from the Zr K edge in $SrZrO_3$, $SrZr_{0.95}Yb_{0.05}O_3$ and $SrZr_{0.9}Yb_{0.1}O_3$ and the Yb $L_{III}$ edge in $Yb_2O_3$ show clear contributions by next-nearest ions at 3.0–4.0 Å, while those from the Yb $L_{III}$ edge in $SrZr_{0.95}Yb_{0.05}O_3$ and $SrZr_{0.9}Yb_{0.1}O_3$ are mainly constructed by a first-nearest signal. Moreover, the nearest Yb–O distributions at 1.0–2.0 Å have a side peak with a strong intensity in both $SrZr_{0.95}Yb_{0.05}O_3$ and $SrZr_{0.9}Yb_{0.1}O_3$. It is shown from the analyses of the side peak that the nearest Yb–O bonds consist of two distances (1.96 and 2.18 Å). Two structural models around the Yb ion have been suggested and discussed from these results.

## 1. Introduction

Protons can be included in interstitial sites of some perovskite-type oxides $ABO_3$, when a few mol% trivalent cations are substituted for $B^{4+}$ ions. Since Iwahara *et al* [1] discovered that the protons exhibit relatively high mobility and give rise to significant proton conduction in $SrCeO_3$, the proton conduction property has been found in various perovskite oxides ($BaCeO_3$ [2, 3], $BaZrO_3$ [2], $SrZrO_3$ [4, 5] and others). These proton conductors show a remarkably high chemical stability with possible applications as solid electrolytes in fuel cells and hydrogen sensors. In addition to those applications, a number of experimental and theoretical works have been performed in order to understand the mechanism of the proton conduction. Schober *et al* [6] determined proton diffusivity in $SrZrO_3$ and $SrCeO_3$ doped with $Yb^{3+}$ by using an electrochemical technique. Their results show that proton diffusivity does not depend so much on the host lattice. On the other hand, the diffusion process was found by quasielastic neutron scattering to consist of a sequence of free diffusion (free state) and trapping events by Yb ions (trapping state) [7]. The dopant ion concentration dependence of the proton conductivity was also reported [8]. It is well accepted that the doped trivalent ion plays an important role in the proton conduction mechanism. Previously, numerical and theoretical calculations have been carried out to simulate proton diffusion and the magnitude of local distortion by proton migration [9–11]. However, these numerical calculations of proton migration were presented in almost ideal host lattice, and did not include the effect of the local structural distortion around

0953-8984/01/112455+12$30.00  

a dopant ion. A comprehensive understanding of an interaction between a host lattice and a dopant ion is still lacking. It is, therefore, necessary to investigate the local structure around the dopant ion experimentally. Extended x-ray absorption fine structure (EXAFS) is a powerful technique to measure the local structure around ions of interest. Recently, Osaka *et al* [12] suggested by EXAFS and x-ray absorption near edge structure (XANES) on $SrZr_{1-x}Yb_xO_3$ that the oxygen vacancy would be localized near the Yb ion, but the local structure around the Yb ion has not been understood well. In this paper, $SrZr_xYb_{1-x}O_3$ ($x = 0.0$, 0.05 and 0.1) have been investigated by using the EXAFS technique and a local structural model around the Yb ion will be discussed.

## 2. Experiment

Single crystals were made by melting using a xenon arc-imaging furnace and single crystal powder was prepared by crushing a bulk crystal in a mortar. The powder was analysed by x-ray powder diffraction to confirm that a single phase product was obtained (space group $Pnma$, $Z = 4$) [13, 14]. Samples of $SrZrO_3$, $SrZr_{0.95}Yb_{0.05}O_3$ and $SrZr_{0.9}Yb_{0.1}O_3$ for the measurements of the Zr K edge and $Yb_2O_3$ for that of the Yb $L_{III}$ edge were prepared by dusting the powders onto tapes. Those of $SrZr_{0.95}Yb_{0.05}O_3$ and $SrZr_{0.9}Yb_{0.1}O_3$ for the measurements of the Yb $L_{III}$ edge were prepared by pressing into a disc mixed with boron nitride (BN) from those powders, because these samples require approximately 0.1 mm thickness due to the low concentration of Yb. EXAFS absorption spectra of the Yb $L_{III}$ edge and Zr K edge were measured at room temperature in the Photon Factory of the National Laboratory for High Energy Physics in Japan (KEK, Tsukuba, Japan). The current of positron storage ring was approximately 300 mA at 2.5 GeV. A monochromatized x-ray beam was provided by a Si(111) double-crystal monochromator at BL-12C for the measurements of the Yb $L_{III}$ edge (8.9 keV) and by a Si(311) channel-cut monochromator at BL-10B for that of the Zr K edge (18.0 keV). Harmonic rejection for the Yb $L_{III}$ edge was accomplished by detuning 70% of the original x-ray intensity and by using a mirror system at BL-12C. Because a mirror system was not installed in the BL-10B facility, higher harmonics could not be removed for the measurements of the Zr K edge. However, the second-order harmonic (36.0 keV) of the Zr K edge was eliminated by the extinction rule and the third-order harmonic (54.0 keV) was hardly included in this synchrotron radiation beam. The incident and transmitted x-ray intensities were measured with ionization chambers filled with an appropriate mixture of Ar and $N_2$ gases.

## 3. Results and discussion

Figure 1 shows x-ray absorption spectra at the Zr K edge and the Yb $L_{III}$ edge at room temperature. Victoreen functions fitted to the pre-edge spectra are also shown in these figures. The EXAFS oscillations, $k^3\chi(k)$, were extracted from the measured absorption spectra following a standard procedure [15, 16] as shown in figure 2. The wavenumber $k$ of the photoelectron is given by $k = \sqrt{(2m/\hbar^2)(E - E_0)}$, where $m$ is the electron mass and $E_0$ is the threshold energy. The programs XAFS93 and MBF93 were employed for the EXAFS data analyses [16]. The Fourier transform of $k^3\chi(k)$ yields a radial structure function $F(R)$:

$$F(R) = \frac{1}{\sqrt{2\pi}} \int_{k_{\min}}^{k_{\max}} w(k)k^3\chi(k) \exp(\mathrm{i}2kR)\,\mathrm{d}k \tag{1}$$

where $w(k)$ is the Hanning window function. The radial structure functions $F(R)$ around (a) Zr in $SrZrO_3$, (b) Yb in $SrZr_{0.95}Yb_{0.05}O_3$, (c) Yb in $SrZr_{0.9}Yb_{0.1}O_3$ and (d) Yb in $Yb_2O_3$ were obtained by a Fourier transform of $k^3\chi(k)$ in the range of 2.00 $\text{Å}^{-1} \leqslant k \leqslant 11.00$ $\text{Å}^{-1}$ as

shown in figure 3. The correction of the phase shift was not taken into account at this stage. The $F(R)$ for $SrZrO_3$ ((a) in figure 3) and $Yb_2O_3$ ((d) in figure 3) show clear contributions from the next-nearest ions at 3.0–4.0 Å, while those from $SrZr_{0.95}Yb_{0.05}O_3$ ((b) in figure 3) and $SrZr_{0.9}Yb_{0.1}O_3$ ((c) in figure 3) are mainly constructed by a first-nearest signal. The decrease of the signal from next-nearest ions corresponds to the decrease in correlation between Yb and next-nearest ions. Such a phenomenon is well known in amorphous materials [17, 18].

The peaks of Abs$[F(R)]$ for all samples at 1.0–2.0 Å are attributed to neighbouring oxygen ions. The Yb–O distributions in both $SrZr_{0.95}Yb_{0.05}O_3$ and $SrZr_{0.9}Yb_{0.1}O_3$ have a side peak with a strong intensity as marked with arrows in figures 3(b) and (c). The origin is ascribed to an overlap of different Yb–O bond lengths. In order to determine the local structural parameters, a non-linear least-squares fitting was carried out by comparing the observed and

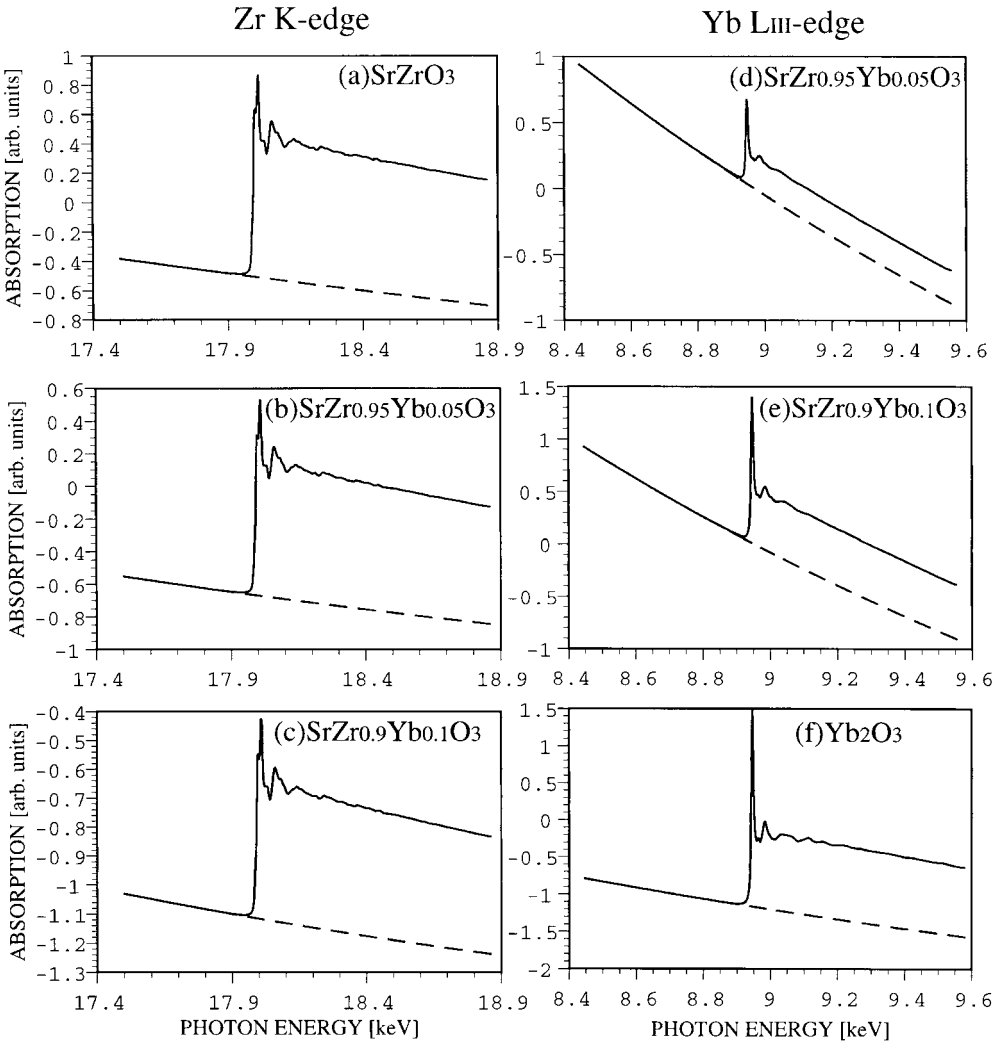


**Figure 1.** X-ray absorption spectra at the Zr K edge, (a) $SrZrO_3$, (b) $SrZr_{0.95}Yb_{0.05}O_3$ and (c) $SrZr_{0.9}Yb_{0.1}O_3$, and at the Yb $L_{III}$ edge, (d) $SrZr_{0.95}Yb_{0.05}O_3$, (e) $SrZr_{0.9}Yb_{0.1}O_3$ and (f) $Yb_2O_3$. The dashed lines are the background absorption extrapolated by a Victoreen function.

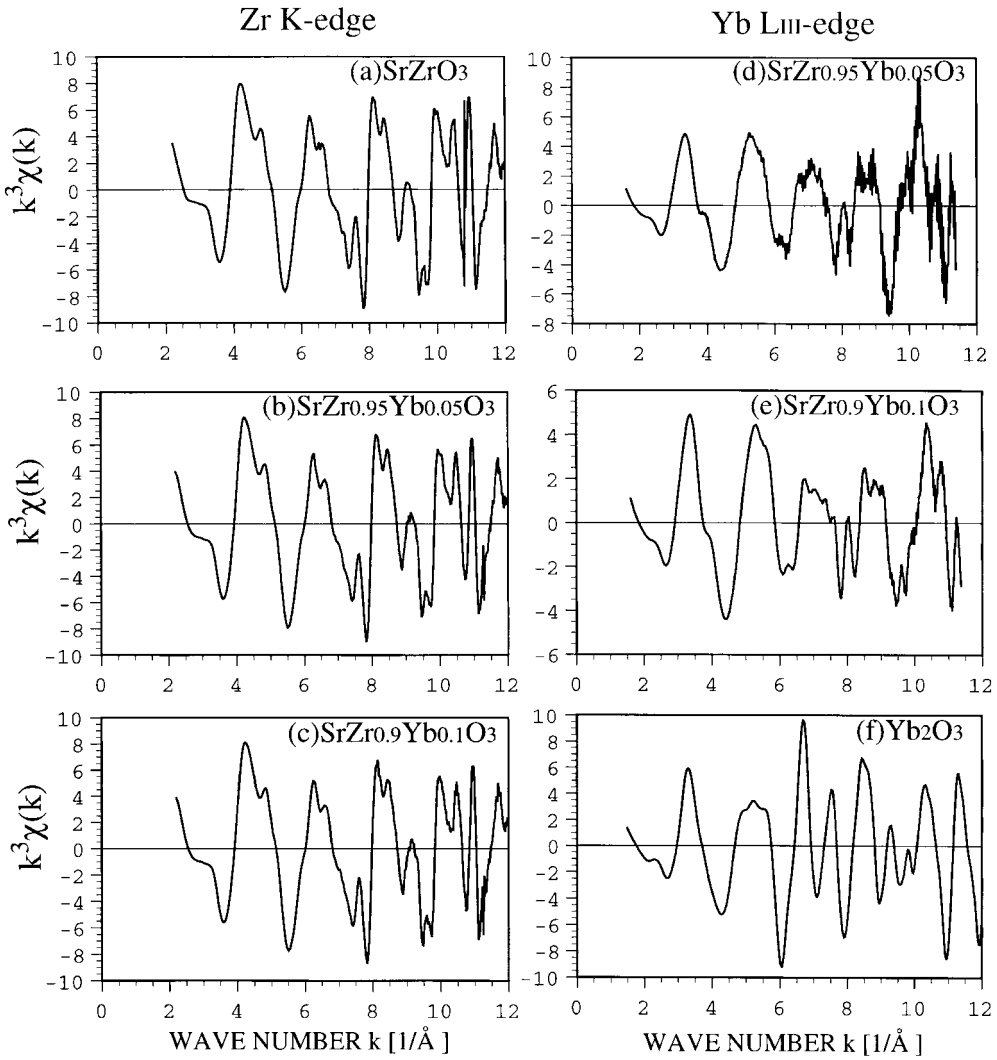


**Figure 2.** $k^3\chi(k)$ at the Zr K edge, (a) $SrZrO_3$, (b) $SrZr_{0.95}Yb_{0.05}O_3$ and (c) $SrZr_{0.9}Yb_{0.1}O_3$ and at Yb $L_{III}$ edge, (d) $SrZr_{0.95}Yb_{0.05}O_3$, (e) $SrZr_{0.9}Yb_{0.1}O_3$ and (f) $Yb_2O_3$ after normalization, background removal and conversion to $k$-space.

calculated $k^3\chi(k)$. We used the EXAFS formula in the single scattering theory with the harmonic approximation [19],

$$k^3\chi(k) = \sum_B \frac{k^2 N_B}{R^2} |f_B(k;\pi)| \exp\left(-\frac{2R}{\lambda(k)}\right) \exp(-2\sigma^2 k^2) \times \sin\left\{2kR - \left(\frac{2k}{R}\right)\left(1 + \frac{2R}{\lambda(k)}\right)\sigma^2 + \delta_{\text{total}}\right\} \tag{2}$$

where $N_B$ is the coordination number of scattering atom B at distance $R$ from the absorbing atom with Debye–Waller factor $\sigma^2$. $|f_B(k;\pi)|$ and $\delta_{\text{total}}$ denote the back-scattering amplitude of photoelectrons and the total phase shift function, respectively. Values of the functions $|f_B(k;\pi)|$ and $\delta_{\text{total}}$ were taken from the theoretical table of Mckale *et al* [20]. The mean free

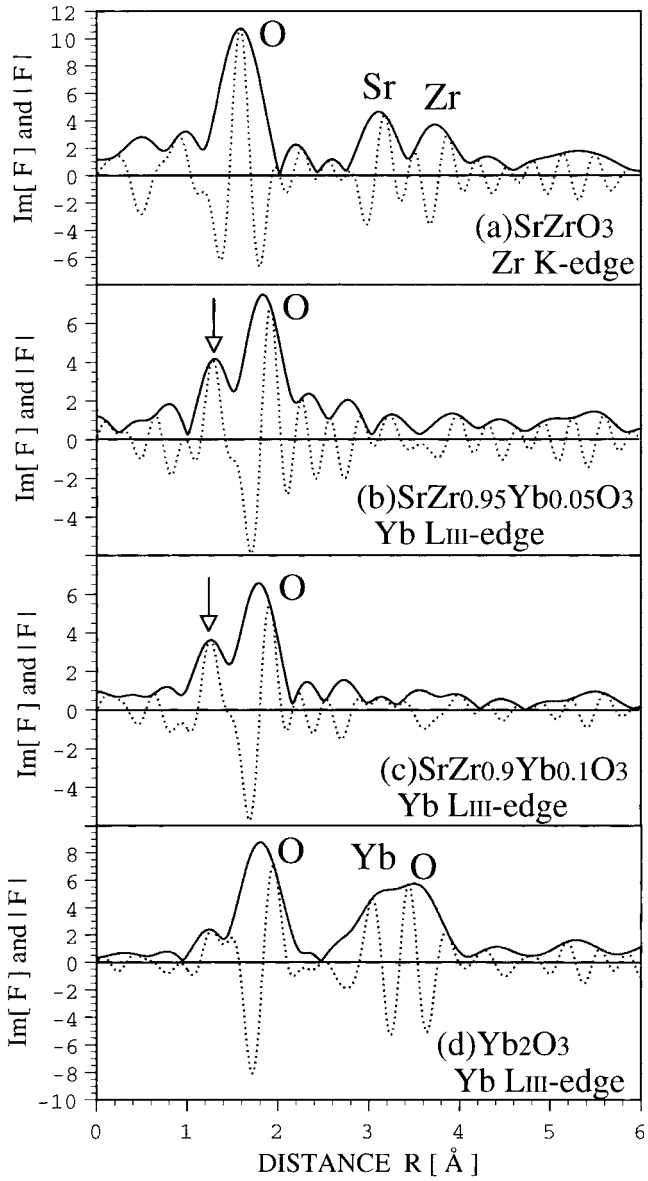


**Figure 3.** Radial structure functions; magnitude (Abs[$F(R)$]: solid curve) and imaginary (Im[$F(R)$]: dotted curve) parts of the Fourier transforms of EXAFS oscillation in the range of $2.00\,\text{Å}^{-1} \leqslant k \leqslant 11.00\,\text{Å}^{-1}$ at room temperature: (a) $SrZrO_3$ at the Zr K edge, (b) $SrZr_{0.95}Yb_{0.05}O_3$ at the Yb $L_{III}$ edge, (c) $SrZr_{0.9}Yb_{0.1}O_3$ at the Yb $L_{III}$ edge and (d) $Yb_2O_3$ at the Yb $L_{III}$ edge.

path $\lambda(k)$ of a photoelectron was assumed to depend on the wavenumber $k$: $\lambda(k) = k/\eta$, where $\eta$ is a constant. In the parameter fitting, according to the EXAFS workshop report [15], we filtered a theoretical EXAFS function in the same way as the observed function to eliminate truncation effects through the Fourier transformation of the data [21]. The Fourier-filtered EXAFS function was obtained by the Fourier transform of the oxygen peak in the range of $1.0\,\text{Å} \leqslant R \leqslant 2.2\,\text{Å}$. The calculations were performed in the range $3.0\,\text{Å}^{-1} \leqslant k \leqslant 11.0\,\text{Å}^{-1}$

on $k^3\chi(k)$. The adjusted parameters were $N_B$, $R$, $\sigma(2)$, $\eta$ and $\Delta E_0$ in equation (2), where $\Delta E_0$ is the correction for the difference between the theoretical and experimental threshold energy. In $SrZr_{0.95}Yb_{0.05}O_3$ and $SrZr_{0.9}Yb_{0.1}O_3$, it was assumed that Yb occupies the Zr site [22, 23] with two types of Yb–O distance (two-shell fitting), because of the observation of the strong side peak. As shown in figure 4, the calculated EXAFS spectra are in agreement with observed ones. The amplitude modulations of the Yb–O EXAFS spectra, which would arise from an overlap of different Yb–O bond lengths, is precisely duplicated. However, there are large discrepancies in the high-$k$ region of EXAFS spectra of $SrZr_{0.95}Yb_{0.05}O_3$ between experimental and calculated values as shown in figure 4(a). It seems that an experimental error due to the dilute nature of the dopants is amplified by $k^3$ as shown in figure 2(d). It is apparent that the amplitude modulation in the high-$k$ region makes the Yb–O distances inequivalent, because the back-scattering amplitude $|f_B(k;\pi)|$ of the oxygen atom is monotonically decreasing above 3.0 $Å^{-1}$. Therefore, we also carried out the Fourier transform in a narrow range of $2.00\ Å^{-1} \leqslant k \leqslant 9.00\ Å^{-1}$ as shown in figure 5, and then the strong side peaks disappeared. Figure 6 shows the comparison between the observed EXAFS spectra and calculated ones on the assumption of a single Yb–O distance (one-shell fitting). Since these Fourier filtered spectra have no amplitude modulation, the observed values could be made to agree with calculated ones by one-shell fitting.

Table 1 gives the obtained local structural parameters around Yb in $SrZr_{0.95}Yb_{0.05}O_3$ and $SrZr_{0.9}Yb_{0.1}O_3$ and in addition the results of the calculations for the first-nearest Zr–O in $SrZrO_3$ and of Yb–O in $Yb_2O_3$ for reference. Here, distances $R$ and coordination numbers $N_B$ of these reference materials are fixed at x-ray diffraction data. The first-nearest Zr–O in $SrZrO_3$ (space group $Pnma$, $Z = 4$) has three different distances of 2.086, 2.094 and 2.096 Å with $N_B = 2$ coordinates at room temperature [13]. Ytterbium oxide $Yb_2O_3$ has a C-rare earth structure (space group $Ia3$, $Z = 16$) [24]. Two kinds of crystallographically different site for Yb ions are coordinated by six oxygen ions in $Yb_2O_3$. One has the same Yb–O bond lengths of 2.245 Å located at the 8b site and the other has the different Yb–O bond lengths of 2.217, 2.233 and 2.286 Å located at the 24d site [25].

The obtained Yb–O distances in the one-shell fitting are approximately 2.21 Å for both $SrZr_{0.95}Yb_{0.05}O_3$ and $SrZr_{0.9}Yb_{0.1}O_3$ as given in table 1. These are nearly the same as the nearest Yb–O distances in $Yb_2O_3$ rather than Zr–O in $SrZrO_3$. The Debye–Waller factors $\sigma^2$ are much larger than the 0.0047(2) $Å^2$ of Zr–O in $SrZrO_3$, where the value of 0.0047(2) $Å^2$ is in good agreement with the 0.0050(5) $Å^2$ reported by the previous study [26]. Moreover, the $\eta$ from the Yb $L_{III}$ edge of $SrZr_{0.95}Yb_{0.05}O_3$ and $SrZr_{0.9}Yb_{0.1}O_3$ are smaller than that from the Yb $L_{III}$ edge of $Yb_2O_3$. Because the $\sigma^2$ and the mean free path $\lambda(k)$, $\lambda(k) = k/\eta$, are amplitude terms in the EXAFS oscillation as given in equation (2), it seems that the large $\sigma^2$ values are directly correlated with the small $\eta$.

In the two-shell fitting, the obtained Yb–O distances are 1.96 and 2.18 Å for both $SrZr_{0.95}Yb_{0.05}O_3$ and $SrZr_{0.9}Yb_{0.1}O_3$. These obtained distances are shorter than that of $Yb_2O_3$ and the average of 1.96 and 2.18 Å is nearly equal to the Zr–O distance ∼2.09 Å of $SrZrO_3$. The double-peaked structures appear at approximately 1.3 and 1.8 Å with the difference 0.5 Å in figures 3(b) and 3(c), whereas the difference in between their calculated values is about 0.2 Å (2.18–1.96 Å). Using these best fit parameters for $SrZr_{0.9}Yb_{0.1}O_3$, the radial structural functions were simulated in conditions of various differences of Yb–O distances. Figure 7 shows the Yb–O radial structure functions on (a) 2.18–2.18 Å, (b) 2.18–2.01 Å, (c) 2.18–1.96 Å, described by the best fit values, (d) 2.18–1.91 Å, (e) 2.18–1.73 Å and (f) 2.18–1.61 Å. It is found that the side peak is generated not by a net distribution but by an interference between EXAFS oscillations from the different Yb–O lengths. If all Yb–O nearest-neighbour distances are the same, a large ripple does not appear on the lower slopes on the Yb–O distribution as

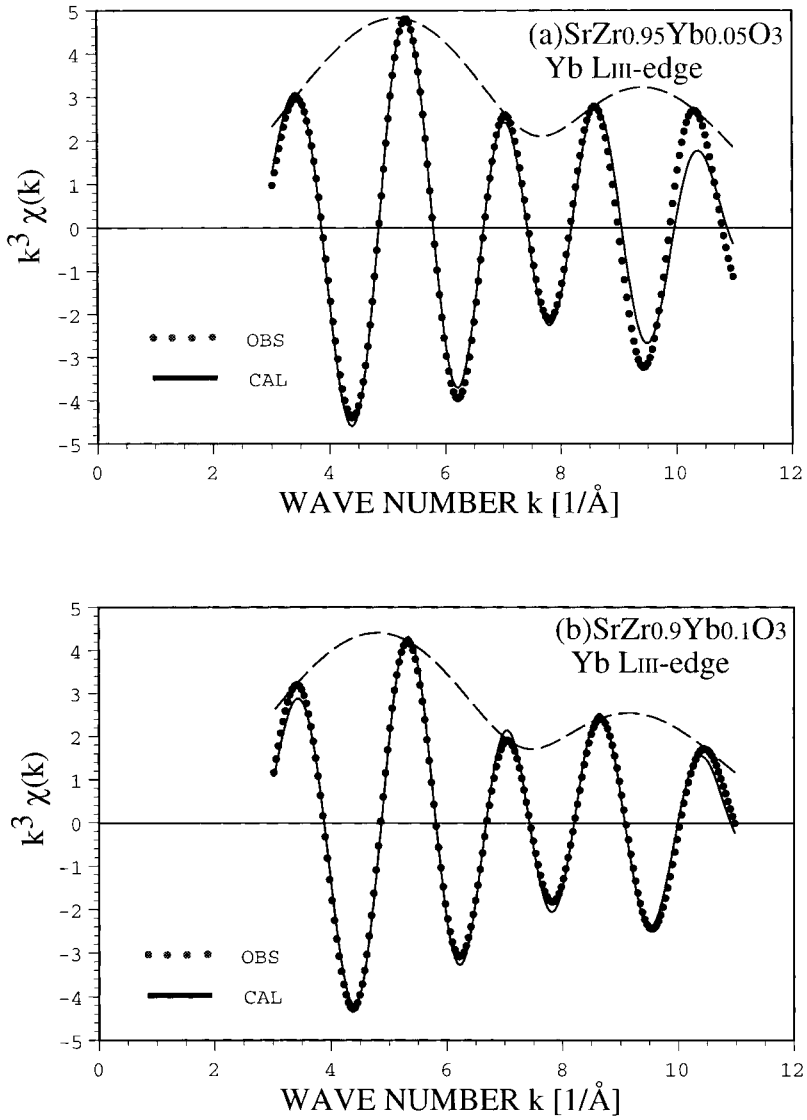


**Figure 4.** Comparisons of an experimental EXAFS spectrum $k^3\chi(k)$ (filled circle) with a calculated one (solid curve) by two-shell fitting for the first-nearest-neighbour O ions around Yb in (a) $SrZr_{0.95}Yb_{0.05}O_3$ and (b) $SrZr_{0.9}Yb_{0.1}O_3$. The dashed curve represents an envelope of the experimental spectrum.

shown in figure 7(a). The values of $\sigma^2$ of the Yb-doped $SrZrO_3$ are smaller than that of $Yb_2O_3$ and are coincident with that of the Zr–O in $SrZrO_3$. The fact that the obtained values of $\eta$ from the Yb $L_{III}$ edge of the Yb-doped $SrZrO_3$ are exactly equal to that from the Yb $L_{III}$ edge of $Yb_2O_3$ will provide more reliable results for the $\sigma^2$. The Yb–O thermal vibration would be restrained by the vicinity of the host lattice $SrZrO_3$. Those two results, that the average of the two kinds of Yb–O distances is nearly equal to the Zr–O distance of $SrZrO_3$ and the $\sigma^2$ agrees with that of $SrZrO_3$, were suggested by the two-shell fitting. This confirms the fact that the Yb ions are substituted for the Zr ions [22, 23].

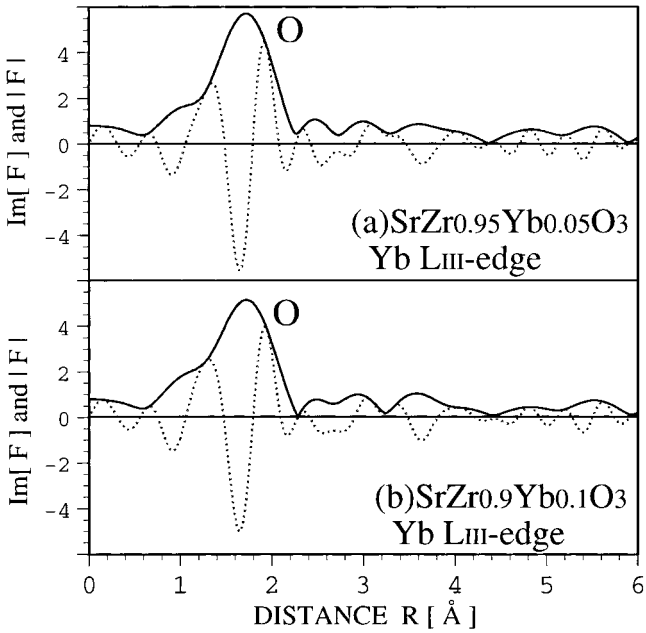


**Figure 5.** Radial structure functions; magnitude (Abs[$F(R)$]: solid curve) and imaginary (Im[$F(R)$]: dotted curve) parts of the Fourier transforms of EXAFS oscillation in the range of 2.00 Å$^{-1}$ $\leqslant k \leqslant$ 9.00 Å$^{-1}$ at room temperature: (a) $SrZr_{0.95}Yb_{0.05}O_3$ and (b) $SrZr_{0.9}Yb_{0.1}O_3$ at the Yb $L_{III}$ edge.

**Table 1.** Local structure parameters of the nearest oxygens around the ions of interest.

| | | $N_B$ | $R$ [Å] | $\sigma^2$[Å$^2$] | $\eta$ [Å$^{-2}$] | $\Delta E_0$ [eV] |
|---|---|---|---|---|---|---|
| $SrZr_{0.95}Yb_{0.05}O_3$ (Yb 5 mol%) Yb $L_{III}$ edge | | | | | | |
| 1 shell | Yb–O | 5.2(2) | 2.209(3) | 0.0155(6) | 0.20(3) | 12.9(4) |
| 2 shells | Yb–O | 1.7(1) | 1.963(3) | 0.0044(3) | 0.44(3) | 6.1(4) |
| | Yb–O | 4.3(1) | 2.184(2) | 0.0044 | 0.44 | 6.1 |
| $SrZr_{0.9}Yb_{0.1}O_3$ (Yb 10 mol%) Yb $L_{III}$ edge | | | | | | |
| 1 shell | Yb–O | 5.8(2) | 2.206(4) | 0.0205(8) | 0.19(3) | 12.4(4) |
| 2 shells | Yb–O | 1.6(1) | 1.957(4) | 0.0047(3) | 0.43(3) | 6.4(4) |
| | Yb–O | 4.0(1) | 2.181(2) | 0.0047 | 0.43 | 6.4 |
| | | $N_B$ (fixed) | $R$ [Å] (fixed) | $\sigma^2$[Å$^2$] | $\eta$ [Å$^{-2}$] | $\Delta E_0$ [eV] |
| $SrZrO_3$ Zr K edge | | | | | | |
| | Zr–O | 2.0 | 2.086 | 0.0047(2) | 0.90(3) | −2.8(3) |
| | Zr–O | 2.0 | 2.094 | 0.0047 | 0.90 | −2.8 |
| | Zr–O | 2.0 | 2.096 | 0.0047 | 0.90 | −2.8 |
| $Yb_2O_3$ Yb $L_{III}$ edge | | | | | | |
| | Yb–O (8b) | 1.5 | 2.245 | 0.0086(3) | 0.43(3) | 11.1(3) |
| | Yb–O (24d) | 1.5 | 2.217 | 0.0086 | 0.43 | 11.1 |
| | Yb–O (24d) | 1.5 | 2.233 | 0.0086 | 0.43 | 11.1 |
| | Yb–O (24d) | 1.5 | 2.286 | 0.0086 | 0.43 | 11.1 |

The Yb ion concentration dependence of the local structure around Zr has also been studied by using samples of $SrZr_{1-x}Yb_xO_3$ ($x = 0.0, 0.05, 0.1$). As shown in figure 8, there

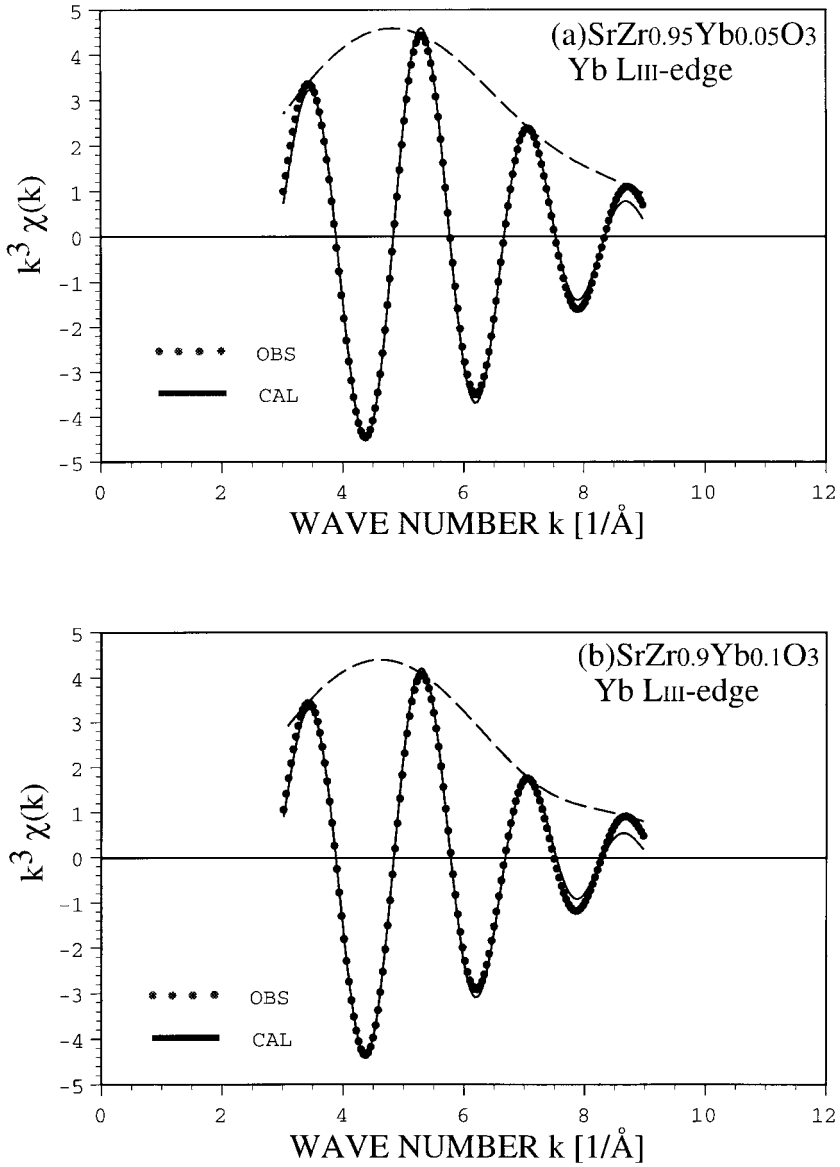


**Figure 6.** Comparisons of an experimental EXAFS spectrum $k^3\chi(k)$ (filled circle) with a calculated one (solid curve) by one-shell fitting in (a) $SrZr_{0.95}Yb_{0.05}O_3$ and (b) $SrZr_{0.9}Yb_{0.1}O_3$. The dashed curve represents an envelope of the experimental spectrum.

was no significant difference among their radial structure functions. When the nearest Zr–O distributions were quantitatively analysed, each of these structural values was the same within the standard deviation. It is of some interest that the dopant Yb ion can have no effect on the local structure around Zr, though the probabilities with which Yb enters the neighbour sites of Zr are 0.3 and 0.6 in $SrZr_{0.95}Yb_{0.05}O_3$ and in $SrZr_{0.9}Yb_{0.1}O_3$, respectively. There must be some changes in the local structure around Zr, when the Yb–O distance is so close to that of $Yb_2O_3$ and the thermal vibration is so strong as obtained by one-shell fitting. However, no

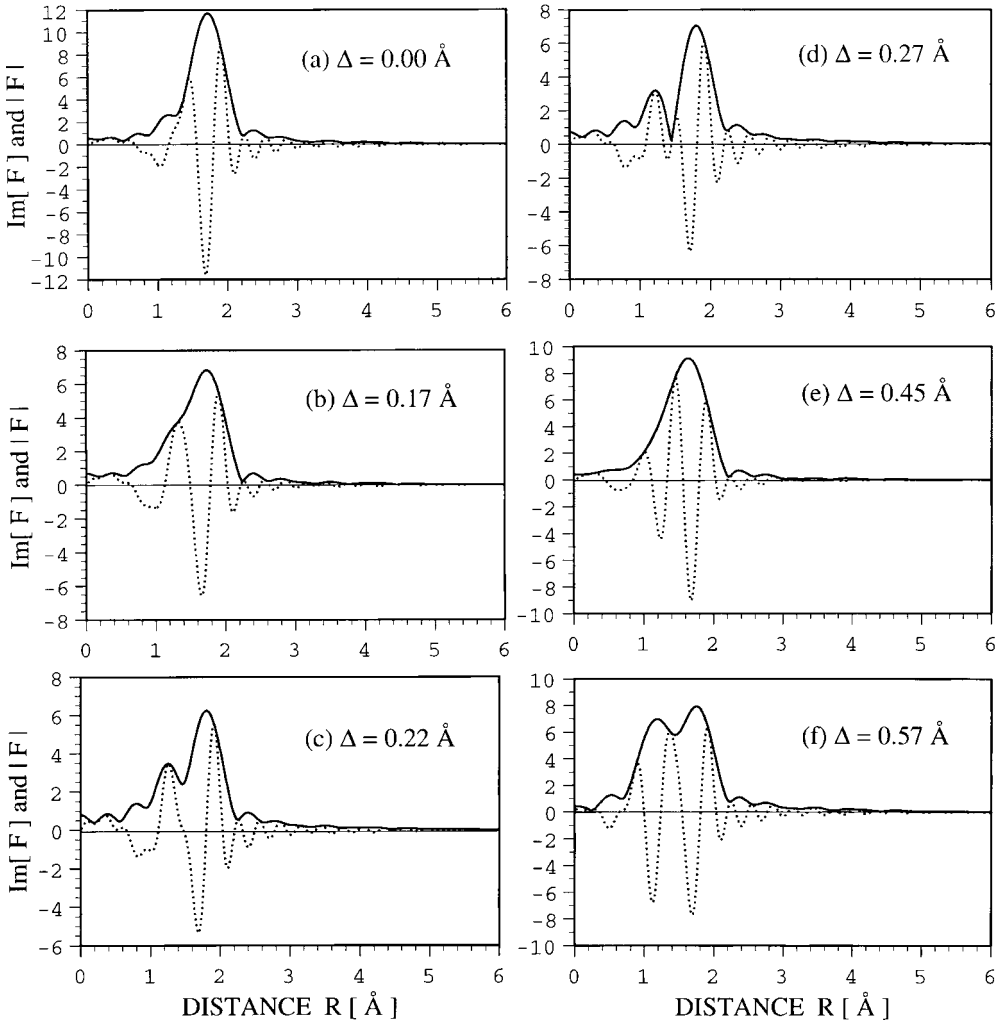


**Figure 7.** Simulation for the Yb–O in *r*-space. These simulations were obtained as described in the text. Δ denotes the difference between two Yb–O distances.

significant change could be observed in the local structure around Zr, as mentioned above. In contrast, the two-shell fitting gave similar structural parameters to those of the host lattice $SrZrO_3$. Consequently, we concluded that the two-shell fitting is reasonable for the local structure around Yb in $SrZr_{1-x}Yb_xO_3$.

The following results are summarized from the above discussion.

(i) The contribution of next-nearest ions to the radial structure function is weak in $SrZr_{0.95}Yb_{0.05}O_3$ and $SrZr_{0.9}Yb_{0.1}O_3$ as compared with in $SrZrO_3$.
(ii) The strong side peaks in $SrZr_{0.95}Yb_{0.05}O_3$ and $SrZr_{0.9}Yb_{0.1}O_3$ were analysed: the nearest Yb–O bonds are based on the existence of two different distances (1.96 and 2.18 Å).

Two types of structural model around Yb will be suggested from these two results.

*Model 1.* An oxygen octahedron around the Yb ion is distorted with the Yb–O distances of 1.96 and 2.18 Å. It can be expected that the distortion of the oxygen octahedron around the

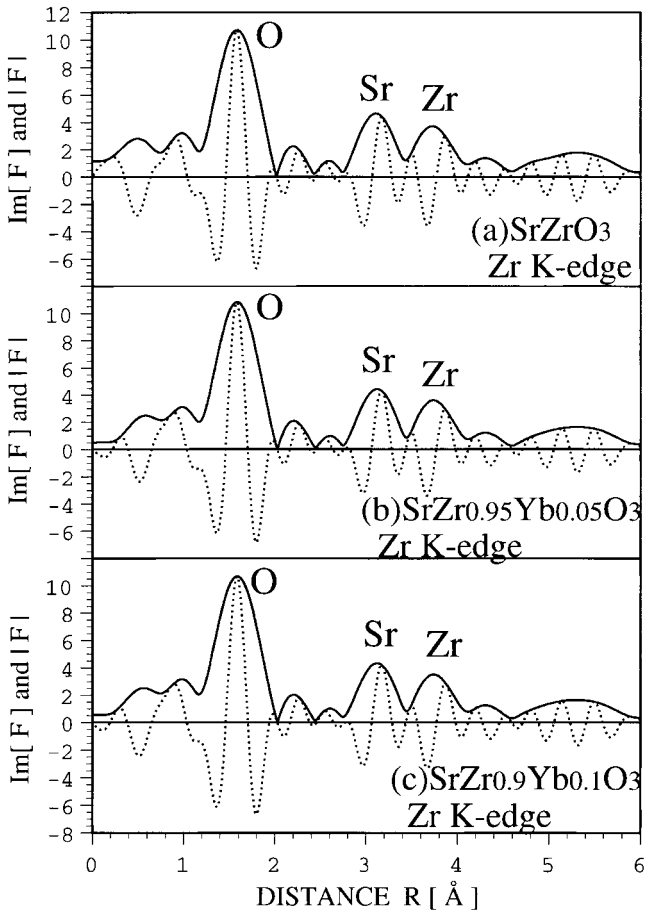


**Figure 8.** Radial structure functions; magnitude (Abs[$F(R)$]: solid curve) and imaginary (Im[$F(R)$]: dotted curve) parts of the Fourier transforms of EXAFS oscillation at room temperature: (a) $SrZrO_3$, (b) $SrZr_{0.95}Yb_{0.05}O_3$ and (c) $SrZr_{0.9}Yb_{0.1}O_3$ at the Zr K edge.

Yb ions will affect the surrounding $SrZrO_3$ host lattice locally. The order of the next-nearest ions around Yb is supposed to be reduced, because of the dispersion of the distances.

Alternatively, an EXAFS technique measures relative correlation between absorption and scattering ions. We cannot distinguish which of absorption or scattering ions are disordered. Then, another explanation would also be possible.

*Model 2*. The Yb ion is located at an off-centre position with the Yb–O distances of 1.96 and 2.18 Å. In this situation, there are various bond lengths between Yb and next-nearest ions. The disorder of Yb will cause the relative position of the next-nearest ions to be disordered, which makes the signals decrease. It is easily seen that model 2 does not induce the lattice distortion as much as model 1. The Yb concentration dependence of the local structure around Zr implies that model 2 may be preferable rather than model 1.

## 4. Conclusion

The local structures around Yb ions in the proton conductor Yb-doped $SrZrO_3$ have been investigated at room temperature by the EXAFS technique. The radial structure functions around Yb of the Yb-doped $SrZrO_3$ show the following significant characters: (i) the decrease of the signal from next-nearest ions and (ii) the strong side peak on the Yb–O distribution, in comparison with those around Zr in $SrZrO_3$ and around Yb in $Yb_2O_3$. The former indicates that the order of the next-nearest ions around Yb is reduced. The latter represents an overlap of different Yb–O bond lengths. Quantitative analyses of the Yb–O bond length evaluated it to be 1.96 and 2.18 Å for both $SrZr_{0.95}Yb_{0.05}O_3$ and $SrZr_{0.9}Yb_{0.1}O_3$. It is found that the local structures around Yb in $SrZr_{0.95}Yb_{0.05}O_3$ and $SrZr_{0.9}Yb_{0.1}O_3$ are quite different from those around Zr in $SrZrO_3$, $SrZr_{0.95}Yb_{0.05}O_3$ and $SrZr_{0.9}Yb_{0.1}O_3$ and around Yb in $Yb_2O_3$.

## Acknowledgments

This work was supported by a Grant-in-Aid for Scientific Research on Priority Areas (12740169) from the Ministry of Education, Science, Sports and Culture of Japan. The authors are grateful to Professor M Nomura and Professor N Usami in the Photon Factory of the National Laboratory for High Energy Physics in Japan. This work was partially supported by CREST of JST (Japan Science and Technology).

## References

[1] Iwahara H, Esaka T, Uchida H and Maeda N 1981 *Solid State Ionics* **3/4** 359
[2] Mitsui A, Miyayama M and Yanagida H 1987 *Solid State Ionics* **22** 213
[3] Scherban T, Lee W K and Nowick A S 1988 *Solid State Ionics* **28/30** 585
[4] Shin S, Huang H H, Ishigame M and Iwahara H 1990 *Solid State Ionics* **40/41** 910
[5] Huang H H, Ishigame M and Shin S 1991 *Solid State Ionics* **47** 251
[6] Schober T, Friedrich J and Condon J B 1995 *Solid State Ionics* **77** 175
[7] Hempelmann R, Karmonik Ch, Matzke Th, Cappadonia M, Stimming U, Springer T and Adams M A 1995 *Solid State Ionics* **77** 152
[8] Yajima T, Suzuki H, Yogo T and Iwahara H 1992 *Solid State Ionics* **51** 101
[9] Shimojo F, Hoshino K and Okazaki H 1996 *J. Phys. Soc. Japan* **65** 1143
[10] Munch W, Seifertli G, Kreuer K-D and Majer J 1996 *Solid State Ionics* **86/88** 647
[11] Matsushita E and Tanase A 1997 *Solid State Ionics* **97** 45
[12] Osaka T, Numako C and Koto K 1999 *Mater. Res. Bull.* **34** 11
[13] Ahtee A, Ahtee M, Glazer A M and Hewat A W 1976 *Acta Crystallogr.* B **32** 3243
[14] Kamishima O, Hattori T, Ohta K, Chiba Y and Ishigame M 1999 *J. Phys.: Condens. Matter* **11** 5355
[15] Lytle F W, Sayers D E and Stern E A 1989 *Physica* B **158** 701
[16] Maeda H 1987 *J. Phys. Soc. Japan* **56** 2777
[17] Bouldin C E, Stern E A, von Roedern B and Azoulay J 1984 *Phys. Rev.* B **30** 4462
[18] Terauchi H, Iida S, Tanabe K, Maeda H, Hida M, Kamijo N, Osamura K, Takasige M and Nakamura T 1983 *J. Phys. Soc. Japan* **52** 3454
[19] Ishii T 1992 *J. Phys.: Condens. Matter* **4** 8029
[20] Mckale A G, Veal B W, Paulikas A P, Chan S K and Knapp G S 1988 *J. Am. Chem. Soc.* **110** 3763
[21] Kamishima O, Ishii T, Maeda H and Kashino S 1997 *Japan. J. Appl. Phys.* **36** 247
[22] Davies R A, Islam M S and Gale J D 1999 *Solid State Ionics* **126** 323
[23] Davies R A, Islam M S, Chadwick A V and Rush G E 2000 *Solid State Ionics* **130** 115
[24] Roth R S and Schneider S J 1960 *J. Res. NBS* **64** A 309
[25] Schleid T and Meyer G 1989 *J. Less-Common Mater.* **149** 73
[26] Petit P E, Guyot F and Farges F 1997 *J. Physique* IV **7** C2 1065